Fully nonlinear solitary wave interaction with a freely floating vertical cylinder

B.Z. Zhou[a], G. X. Wu[a,b*], Q.C. Meng[b]

[a] College of shipbuilding engineering, Harbin Engineering University, Harbin, China (zhoubinzhen@hrbeu.edu.cn)

[b] Permanent address: Department of Mechanical Engineering, University College London, Torrington Place, London WC1E 7JE, UK (author for correspondence: g.wu@ucl.ac.uk)

Highlights:

- A higher order BEM for the potential flow problem with fully nonlinear conditions on the moving boundary is developed.
- Interaction of fully nonlinear solitary wave with a freely floating body is simulated.

1. Introduction

The present work aims to shed some lights on how a nonlinear transient wave will interact with a freely floating structure, as this is believed to be the main cause for ringing of a TLP or GBS. We shall use a vertical cylinder in solitary wave as an example. There has been extensive research on the propagation of the solitary wave, based on KdV equations with first, second, third and higher order theories, as well as the fully nonlinear theory [1]. For its interaction with a stationary body, Zhao et al. [2] carried out numerical simulations wave scattering by a circular cylinder group using the FEM. Cao & Wan [3] took into account the viscosity of the fluid and used the Reynolds-Average Navier-Stokes (RANS) model. For interaction of solitary wave with a free floating body, Isaacson [4] considered a vertical cylinder. However, only very limited results were given and only vertical motion was considered.

In the present work, an initially vertical cylinder is placed in the wave and it will be free to respond to wave excitation in multi degrees of freedom. The accuracy of the present numerical model is verified by comparing wave propagation of a solitary wave with the fully nonlinear solution from [1]. Simulations are then made for solitary wave interaction with a truncated cylinder.

2. Mathematical model and numerical procedure

We consider the problem of wave interaction with a vertical cylinder in water of depth d. Two right-handed Cartesian coordinate systems are defined. One is the space-fixed system *oxyz* with the *oxy* plane on the undisturbed free surface and the *z*-axis pointing upwards. The other is a body-fixed system *o'x'y'z'* with its origin *o'* placed at the centre of mass of the body. These two sets of coordinate systems are parallel to each other when the body is at its equilibrium position. The centre of mass is located initially at $\mathbf{X}_{c0}$ in the space-fixed coordinate system, and $\mathbf{X}_c(=\mathbf{X}_{c0}+\boldsymbol{\zeta})$ subsequently. Here $\boldsymbol{\zeta}=(\zeta_1, \zeta_2, \zeta_3)$ denotes the translational displacements of the mass centre in the *x*, *y* and *z* directions respectively. The rotation of the body is defined through the usual Euler angles $\boldsymbol{\theta}=(\alpha, \beta, \gamma)=(\zeta_4, \zeta_5, \zeta_6)$, to illustrate rotational displacement about *x'*, *y'* and *z'* directions respectively.

Based on the assumption that the fluid is ideal and incompressible, and flow is irrotational, the velocity potential $\phi(x, y, z, t)$ satisfies the Laplace equation in the fluid domain *R*

$$\nabla^2\phi = 0 \tag{1}$$

At the side surface S_C of the computational domain, the seabed surface S_D and the far left and right surfaces S_R in the direction of the incident wave, the impermeable condition is given, or $\partial\phi/\partial n=0$. On the free surface S_F, the fully nonlinear kinematic and dynamic boundary conditions can be given in the following Lagrangian form

$$\frac{D\mathbf{X}}{Dt} = \nabla\phi \tag{2}$$

$$\frac{D\phi}{Dt} = -g\eta + \frac{1}{2}\nabla\phi\cdot\nabla\phi \tag{3}$$

where *g* represents the acceleration due to gravity, $\mathbf{X}=(x, y, z)$ denotes the position vector of a fluid particle on the free surface, η is the elevation of water surface measured from its mean level, $D/Dt=\partial/\partial t+\mathbf{u}\cdot\nabla$ is the total derivative with $\mathbf{u}$ being the velocity of the fluid particle. The boundary condition on the body surface S_B is

$$\frac{\partial\phi}{\partial n} = \mathbf{V}\cdot\boldsymbol{n} \tag{4}$$

where **V** is the velocity of the body surface, **n** is the normal of the surface pointing out of the fluid domain. The body surface velocity can be expanded as

$$\mathbf{V} = \mathbf{U} + \boldsymbol{\Omega} \times \mathbf{r}_b \tag{5}$$

where $\mathbf{r}_b=\mathbf{X}'$ is the position vector in the body-fixed coordinate system, $\mathbf{U}=d\boldsymbol{\zeta}/dt=(U_1, U_2, U_3)$ is the translational velocity of the centre of mass, $\boldsymbol{\Omega}=(U_4, U_5, U_6)$ is the rotational velocity.

The undisturbed solitary wave [1] is used at far upstream of the body as the boundary condition, where the disturbed potential can be assumed to have not arrived. Some auxiliary functions ψ_i (i=1, …, 6) are introduced to decouple the nonlinear fluid-structure interaction problem. These functions satisfy the Laplace equation in the fluid domain. They are zero on the free surface and their normal derivatives $\partial\psi_i/\partial n=n_i$ on the body surface and are zero on the other rigid boundaries. Through the use of these functions, the equation of motion can be written as [5]

$$\sum_{j=1}^{6}(m_{i,j}+c_{i,j})a_j = Q_i - m_{33}g\delta_{i,3} + f_{ei} \tag{6}$$

where

$$c_{i,j} = \rho\iint_{S_B}\psi_i n_j \mathrm{d}s \tag{7}$$

$$Q_i = \rho\iint_{S_B}\left[\nabla\psi_i\left[(\mathbf{U}+\boldsymbol{\Omega}\times\mathbf{r}_b)\cdot\mathbf{n}\right]\cdot\left[\nabla\phi-(\mathbf{U}+\boldsymbol{\Omega}\times\mathbf{r}_b)\right]+\psi_i(\boldsymbol{\Omega}\times\mathbf{U})\cdot\mathbf{n}\right]\mathrm{d}s$$

$$-\rho\iint_{S_B+S_F}(gz+\frac{1}{2}|\nabla\phi|^2)\frac{\partial\psi_i}{\partial n}\mathrm{d}s \tag{8}$$

$m_{i,j}$, $m_{i+3,j+3}$, i, j=1, 2, 3 in Eq.(6) are mass and rotational inertias, $\delta_{i,j}=1(i=j)$ and $\delta_{i,j}=0(i\neq j)$ and f_{ei} are the external force and moment.

The higher-order boundary element method is used to solve the mixed boundary value problem described above at each time step. The boundary surface is discretized by the higher-order elements based on quadratic shape functions. After solving the boundary value problem and obtaining the fluid velocities on the free surface, the 4th-order Runge-Kutta scheme is adopted to advance the fully nonlinear free surface boundary conditions in time. For the case without the body, mesh can be generated based on the conventional orthogonal elements. For the case with the body, the mesh on the free surface can be divided into several parts. The element distribution far away from the body is generated by the conventional orthogonal grid. The mesh near the body is generated based on the elliptic differential equations in each part. In the Lagrangian form of the free surface boundary condition, the nodes of elements move both horizontally and vertically. It is possible that elements become distorted as time progresses. When the overall fluid boundary does not change significantly, mesh rearrangement on the free surface is implemented by adopting the spring analogy method to obtain the horizontal coordinates of new nodes on the free surface. Those nodes on the intersections with the body surface and the boundary are treated separately. Interpolation is then used to update the vertical coordinates as well as the potential at each new node. The details can be found in Zhou et al. [6] and Zhou & Wu [7].

3. Numerical results

The water depth d, acceleration due to gravity g and fluid density ρ are used for nondimensionalisation. It means that the velocity is nondimensionalised by $(gd)^{1/2}$, time by $(d/g)^{1/2}$ and pressure by ρgd. $\tau=t/(d/g)^{1/2}$ is introduced to represent the nondimensional time.

The propagation of a single solitary wave is considered for comparison. The total length of the computational domain is taken as L=35. The half of the width is W=0.4. The initial wave crest is located at the origin of the space fixed coordinate system. The distance between the left inlet boundary and the origin of the coordinate system is L_{left}=15, and that between the right outlet boundary and the origin is L_{right}=20.

The special and time convergence study is carried out and then the element size is chosen as $\Delta x=\Delta y$=0.4 on the free surface, and three elements are specified and nodes are distributed uniformly in the vertical direction of boundaries away from the body. The time step is considered as $\Delta\tau$=0.04. Fig.1 shows the results for the case of ε=0.5, where $\varepsilon=H/d$, with H being the wave height. It can be seen that the present simulation gives graphically identical result to that of Clamond & Dutykh [1] as τ increases when the solution of Clamond & Dutykh [1] is used as the initial condition. However, when the third order solution [8] is adopted as the initial condition at τ=0, the wave height obtained from the present simulation decreases and the waveform becomes wider during propagation, and a dispersive tail can be observed behind the wave peak.

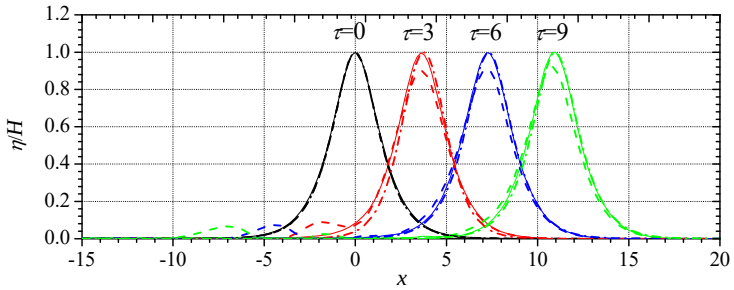

Fig.1. A comparison of free surface profiles. Solid lines and dashed lines are present results using the fully nonlinear solution and the third order solution as the initial condition respectively, and dash dotted lines are solutions of Clamond & Dutykh [1]

A freely floating truncated cylinder of radius R=1.5875 and draught B=0.5 is then placed in the wave with its axis coinciding with the z axis. The mass of the body m is defined as its initial displacement, i.e., m=3.9586. The centre of the mass is located on the axis of the cylinder at z=0.0 when it is in the equilibrium position. The rotation inertial about y' is I_y=2.5766. L=70 and W=15.0 is chosen. The distance between the left inlet boundary and the axis of the cylinder is L_{left}=30. The initial wave crest is placed at x=-15.0. Away from the body, the element size is taken as 0.4 in the horizontal direction. Twenty quadratic elements are used on the half of the cylinder in the circumferential direction and four in the vertical direction. The time interval $\Delta\tau$=0.04 is used.

Fig. 2 present the translations in x and z, as well as rotation about y' for the incoming wave with ε=0.4. A large drift motion in the x direction can be seen because there is no restoring force in this mode. In addition, a relatively small oscillatory motion is also visible. In the vertical direction, the body is first lifted up with a relatively large peak. Due to the fact that there is a restoring force in the vertical direction as a result of the difference in the weight and buoyancy, the motion undergoes several cycles of oscillation. In the rotation about y', the oscillatory motion is most obvious. Although all the motions decrease with time as the solitary wave passes away, the motion in pitch is more persistent and its decay is at a much slower rate. This is because the disturbance of the rotation on the free surface is relatively small when the rotation centre is on the mean free surface. Thus the radiation damping coefficient in rotation about y' is relatively small compared with those in translations in the x and z directions, as has been noticed in [9]. As a result, the decay in rotation about y' is much slower than that in the other two modes.

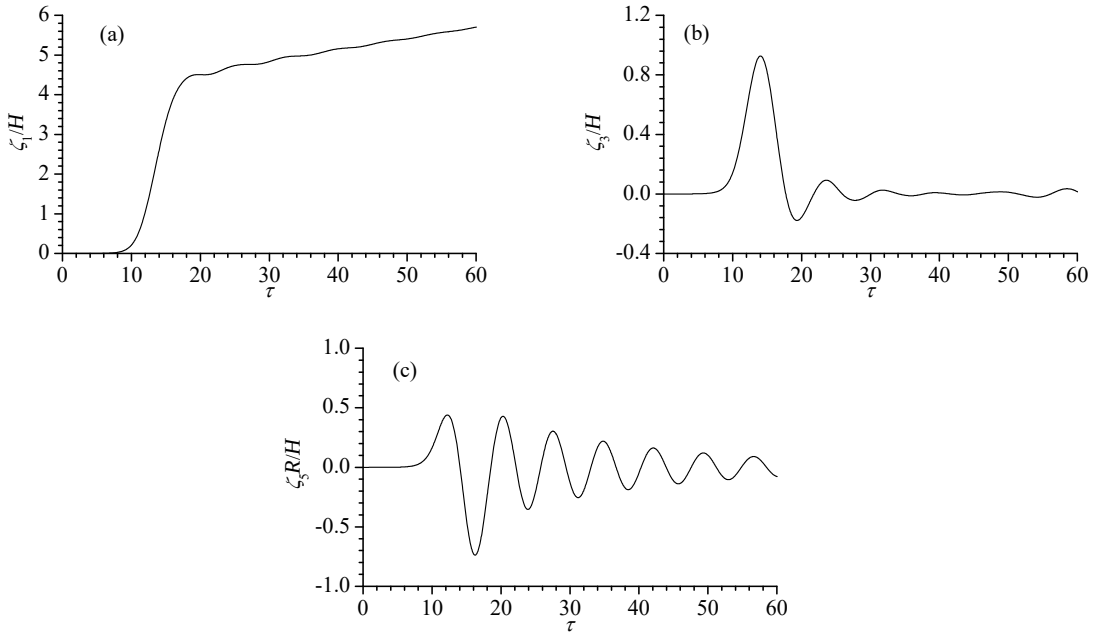

Fig. 2. Time history of motions of the floating truncated cylinder for ε=0.4: (a) displacement in x direction; (b) displacement in z direction and (c) rotation displacement about y'

Fig. 3 shows the forces and moment for the fixed cylinder and the moving cylinder. The loading in the case of moving body is smaller than that on the fixed body. That is because the body response through motion will in general 'soften' the incoming wave force compared with the fixed body, as a result, the wave loading is usually reduced. However, it should

be noted that the body motion and the incoming wave can be out of phase in some cases. The body can move towards the wave during its motion and the force for a freely floating cylinder can be bigger than that on the fixed cylinder. From Fig. 3(c), it can be seen that the moment decays to zero faster after the wave has passed the fixed cylinder, while it oscillates for a longer period of time for the moving body due to the oscillatory rotational motion in Fig. 2(c). Further analysis and results will be provided at the Workshop.

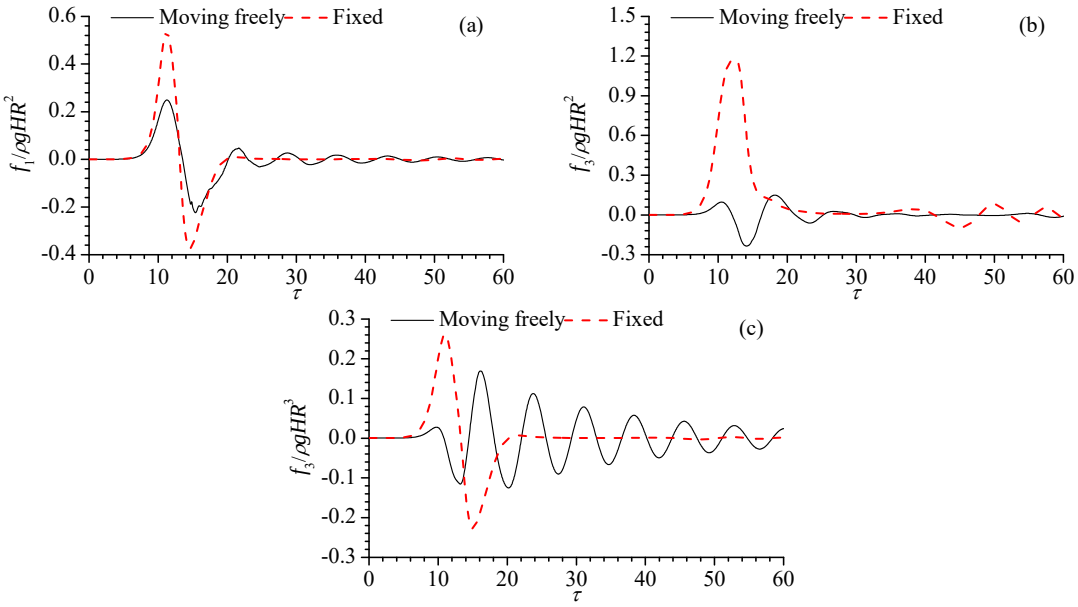

Fig. 3. Time history of wave forces and moment of the floating truncated cylinder for ε=0.4: (a) horizontal force; (b) vertical force and (c) moment about y-axis

Acknowledgement

The authors gratefully acknowledge the financial support from the Lloyd's Register Foundation (LRF) through the joint centre involving University College London, Shanghai Jiaotong University and Harbin Engineering University. The LRF helps to protect life and property by supporting engineering-related education, public engagement and the application of research. This work is also supported by the National Natural Science Foundation of China (11472088, 51409066).

References

[1] Clamond D, Dutykh D. Fast accurate computation of the fully nonlinear solitary surface gravity waves. Comput Fluids 2013; 84: 35-8.

[2] Zhao M, Cheng L, Teng B. Numerical simulation of solitary wave scattering by a circular cylinder array, Ocean Eng 2007; 34(3-4): 489-99.

[3] Cao HJ, Wan DC. RANS-VOF solver for solitary wave run-up on a circular cylinder. China Ocean Eng 2015; 29(2): 183-96.

[4] Isaacson MDSQ. Nonlinear-wave effects on fixed and floating bodies. J Fluid Mech 1982; 120: 267-81.

[5] Wu GX, Eatock Taylor R. The coupled finite element and boundary element analysis of nonlinear interactions between waves and bodies. Ocean Eng 2003; 30: 387-400.

[6] Zhou BZ, Wu GX, Teng B. Fully nonlinear wave interaction with freely floating non-wall-sided structures. Eng Anal Bound Elem 2015; 50: 117-132.

[7] Zhou BZ, Wu GX. Resonance of a tension leg platform exited by third-harmonic force in nonlinear regular waves. Phil Trans R Soc 2015; A373: 20140105.

[8] Grimshaw R. The solitary wave in water of variable depth. Part 3. J Fluid Mech 1971; 46: 611-22.

[9] Zhou BZ, Teng B. Numerical investigation of wave radiation by a vertical cylinder using a fully nonlinear HOBEM. Ocean Eng 2013; 70: 1-13.